Journal of Materials Chemistry A

RSC Publishing

PAPER

View Article Online
View Journal | View Issue

Cite this: *J. Mater. Chem. A*, 2013, **1**, 7174

Nucleation-limited fullerene crystallisation in a polymer–fullerene bulk-heterojunction blend†

Camilla Lindqvist,[a] Anke Sanz-Velasco,[b] Ergang Wang,[a] Olof Bäcke,[c] Stefan Gustafsson,[c] Eva Olsson,[c] Mats R. Andersson*[a] and Christian Müller*[a]

Received 11th March 2013
Accepted 15th April 2013

DOI: 10.1039/c3ta11018d

www.rsc.org/MaterialsA

The nucleation and growth kinetics of fullerene crystals in thin films of a polymer:fullerene bulk-heterojunction blend are investigated. We find that both processes are strongly diffusion-limited at 100–110 °C due to the proximity to the glass transition temperatures of the blend components. Whereas the growth rate exponentially increases with temperature up to 230 °C, the nucleation rate displays a broad maximum around 150–170 °C, which coincides with the highest rate of fullerene crystallisation. A time-temperature-transformation (TTT) diagram reveals that across the investigated range of temperatures the low rate of nucleation is responsible for the formation of micrometre-sized crystals, which can be detrimental for polymer solar cells. Thus, we identify the lack of sufficient nucleation, which predominantly occurs on the substrate interface, as the origin of this important degradation mechanism.

1 Introduction

Bulk-heterojunction blends of donor and acceptor molecules are widely considered to be the most promising architecture to realise efficient organic solar cells.[1–3] The chemical structure of the donor material can be varied significantly and small molecules, oligomers as well as polymers have been used successfully. In contrast, all high-performance devices rely on the same class of acceptors: fullerenes. One of the most widely employed fullerene derivatives is [6,6]-phenyl-C_{61}-butyric acid methyl ester (PCBM, Fig. 1a). PCBM can be processed from common organic solvents, which typically leads to largely amorphous films that crystallise only when heated above the high glass transition temperature of PCBM, $T_g^{PCBM} \sim 110$–140 °C.[4–6] This tendency to vitrify persists in bulk-heterojunction blends, especially if the donor material is a polymer.

For semi-crystalline donor polymers such as poly(3-hexylthiophene) (P3HT), thermal annealing is the established route to optimise the photovoltaic performance. Crystallisation of P3HT and PCBM leads to the formation of a fine-grained nanostructure.[7–10] A further advantage of such crystalline–crystalline bulk-heterojunctions is the high degree of operational stability since the nanostructure assumes a metastable conformation that is resistant to further phase separation when exposed to elevated temperatures around 85 °C, which some standard solar cell testing procedures demand.[11] Instead, bulk-heterojunction blends that are based on non-crystalline donor polymers such as for instance the poly(phenylene vinylene) copolymer MDMO-PPV or the polyfluorene copolymer APFO3 tend to suffer from a continuous coarsening of the nanostructure when annealed above the glass transition temperature of the blend T_g^{blend}, which usually leads to a detrimental decrease in the photovoltaic performance.[6,12] Often, an increase in phase separation is accompanied by the formation of PCBM crystals that are several micrometres to millimetres in size although the presence of device electrodes confines growth to some extent.[13,14] Moreover, PCBM crystals are surrounded by a distinct polymer-rich depletion zone.[15–18] Without doubt the formation of macroscopic PCBM crystals represents a significant degradation mechanism for polymer solar cells. A clear understanding of PCBM crystallisation is required in order to design means to limit the size of PCBM crystals to dimensions that are more comparable to the thickness of the active layer, *i.e.* 100 nm.

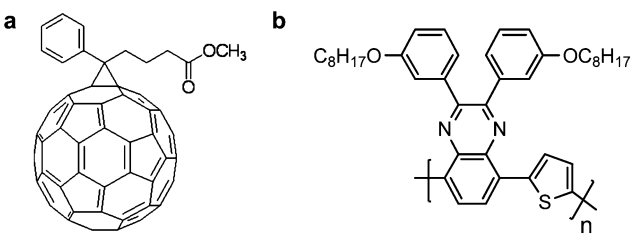

Fig. 1 Structure of (a) PCBM and (b) TQ1.

[a]*Department of Chemical and Biological Engineering/Polymer Technology, Chalmers University of Technology, 41296 Göteborg, Sweden. E-mail: mats.andersson@chalmers.se; christian.muller@chalmers.se*

[b]*Department of Microtechnology and Nanoscience - MC2, Chalmers University of Technology, 41296 Göteborg, Sweden*

[c]*Department of Applied Physics, Chalmers University of Technology, 41296 Göteborg, Sweden*

† Electronic supplementary information (ESI) available. See DOI: 10.1039/c3ta11018d

However, to date the kinetics of PCBM crystallisation in polymer:PCBM bulk-heterojunction blends have not been investigated systematically. A limited number of studies exist that explore the rate of PCBM crystallisation in P3HT:PCBM blends but fail to distinguish between nucleation and growth effects.[4,19–21] Currently, the lack of detailed knowledge about the interplay of PCBM nucleation and growth dynamics complicates the design of optimum processing protocols that permit control of the number and size of PCBM crystals, respectively. Separation of these aspects will aid the preparation of nanostructures with increased thermal stability.

Hence, in this study we explore the kinetics of PCBM crystal nucleation and growth in a bulk-heterojunction blend that comprises the easily synthesised copolymer poly[2,3-bis-(3-octyloxyphenyl)quinoxaline-5,8-diyl-*alt*-thiophene-2,5-diyl] (TQ1, Fig. 1b). We chose to work with TQ1 because it offers a promising photovoltaic performance of up to 5% when blended with PCBM[22] and a reasonably high $T_g^{TQ1} \sim 100$ °C.[23] In addition, we have found that TQ1 does not crystallise.[24] In particular, we explore the number and size of PCBM crystals across a wide range of annealing conditions. To rationalise our observations we employ the classical nucleation and growth theory and construct a time-temperature-transformation (TTT) diagram to illustrate our findings. Thus, we are able to identify nucleation as the rate-limiting step of PCBM crystallisation in TQ1:PCBM blends.

2 Results and discussion

In a first series of experiments we studied the phase behaviour of TQ1:PCBM blends in order to establish over which range of temperatures PCBM crystallisation is likely to occur. We chose a blend composition of 1 : 1 TQ1:PCBM by weight. Differential scanning calorimetry (DSC) was performed between 0 and 295 °C.[25] In this range, second heating thermograms of TQ1 display no thermal transitions, whereas scans of PCBM clearly reveal a double-peak melting endotherm with an end-melting temperature $T_m^{PCBM} \sim 292$ °C, which is typical for this material (Fig. 2a).[5,10] The 1 : 1 blend displays a clear PCBM melting endotherm with only slightly reduced $T_m^{PCBM} \sim 287$ °C. The reduction in end-melting temperature $\Delta T_m^{PCBM} \sim 5$ °C is low compared to other systems based on donor polymers such as P3HT and APFO3.[5,6,26] Thus, we conclude that the miscibility of PCBM and TQ1 is relatively low. Intriguingly, we observe an additional exothermic peak at 175 °C. This re-crystallisation implies that during the preceding cooling scan PCBM crystallisation was not complete and thus continued during the second heating scan. We were unable to deduce the glass transition temperature of the pure components or the TQ1:PCBM blends from the DSC scans. Therefore, we followed the growth of PCBM crystals during heating by measuring the transmittance of blend films between discrete isothermal annealing steps of 300 s. In the transparent region, *e.g.* at 760 nm (*cf.* ESI Fig. S1†), the change in transmittance can be assigned to light scattering of PCBM crystals, as previously reported.[27,28] We find that the transmittance decreases above 110 °C and thus deduce a T_g^{blend} slightly below 110 °C (Fig. 2b).

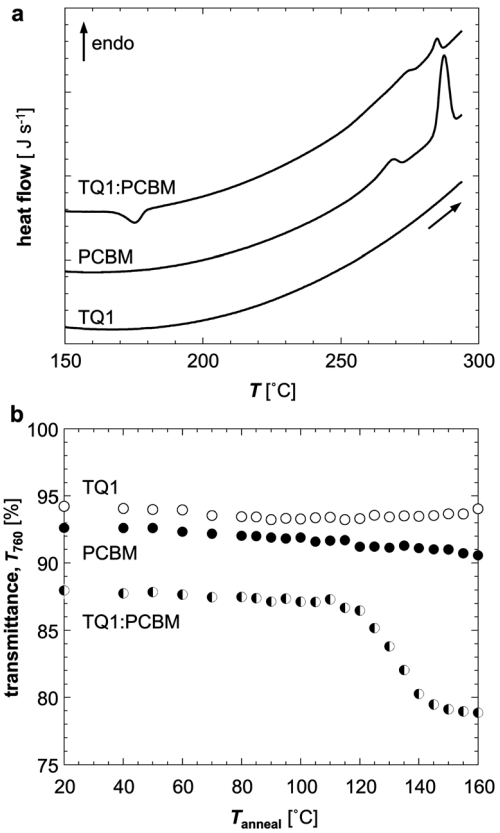

Fig. 2 (a) DSC heating scans of 1 : 1 TQ1:PCBM, PCBM and TQ1, respectively, and (b) change in transmittance at 760 nm as a function of annealing temperature of TQ1 (open circles), PCBM (filled circles) and 1 : 1 TQ1:PCBM (half-filled circles).

This observation is in good agreement with literature values for the two blend components, $T_g^{PCBM} \sim 110$–140 °C[4–6] and $T_g^{TQ1} \sim 100$ °C.[23]

PCBM crystallisation can be expected to proceed at temperatures $T_g < T < T_m$. Thus, we studied the nucleation and growth of PCBM crystals in the temperature range of 110 to 230 °C. We used optical microscopy to examine 90 nm thick TQ1:PCBM thin films in between discrete isothermal annealing steps that were performed at ambient atmosphere but in the absence of light, in order to avoid thermal degradation.[29] Verploegen *et al.* and He *et al.* have argued that in spin-coated thin films PCBM crystals nucleate on the substrate.[4,20] Thus, initially we studied the effect of different substrates. We noticed that the type of substrate has a pronounced influence on the number but not size of crystals, which indicates that nucleation is sensitive to the surface properties. For instance, as displayed in Fig. 3 glass substrates resulted in a considerably higher crystal density than PEDOT:PSS coated glass substrates. We measured both, the water contact angle and the root mean squared surface roughness of our substrates and obtained values of 25° and 2.5 nm for glass whereas PEDOT:PSS yielded 18° and 0.8 nm. In contrast, TQ1 and PCBM with water contact angles of 83° and 71°, respectively, are considerably more hydrophobic. He *et al.* have pointed out that the choice of substrate, *i.e.* glass or PEDOT:PSS, can influence the composition at the substrate interface, which may influence PCBM nucleation.[20] In addition, we note that the

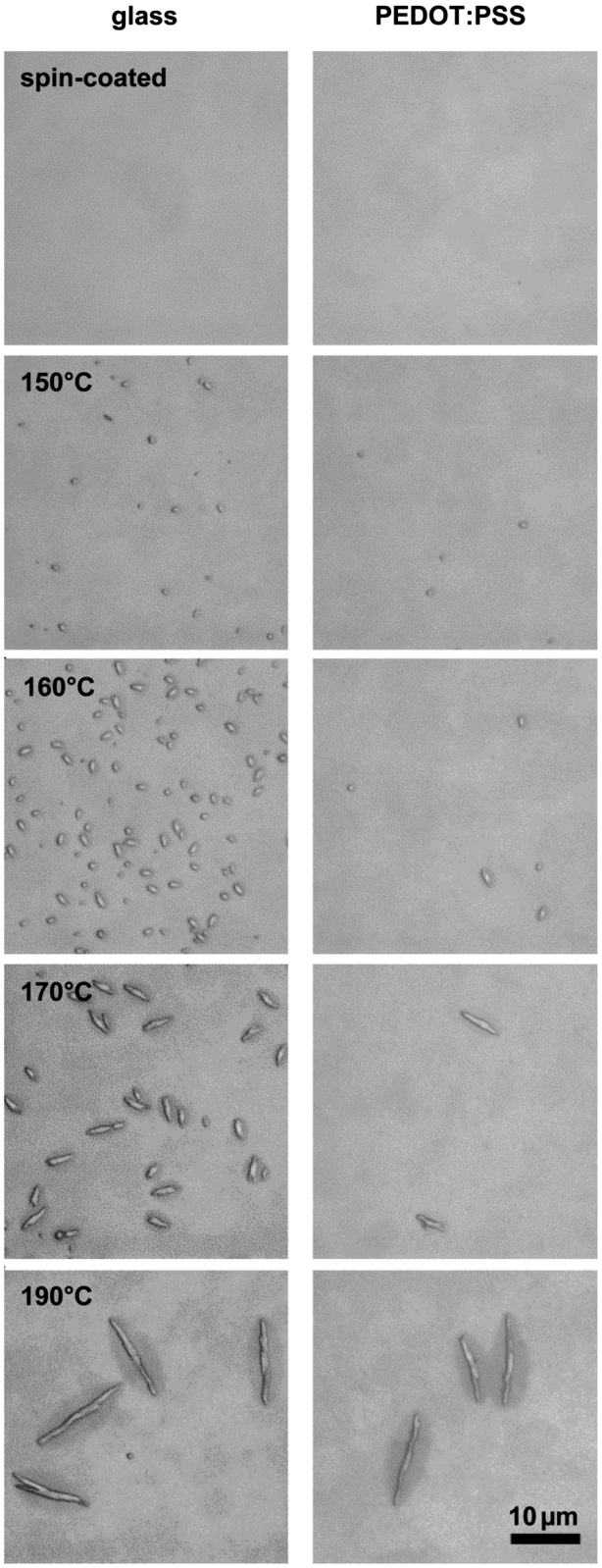

Fig. 3 Optical micrographs of 1 : 1 TQ1:PCBM spin-coated on glass (left column) and PEDOT:PSS coated glass (right column) that was annealed for 180 s at the indicated temperatures.

glass substrates used in this study feature a considerably higher surface roughness, which may offer more nucleation sites that can initiate growth of PCBM crystals.

The smallest PCBM crystals that can be resolved with optical microscopy are approximately 0.5 μm large. In order to determine if smaller crystallites are present, we also studied TQ1:PCBM films with transmission electron microscopy (TEM) and scanning electron microscopy (SEM). TEM studies of a spin-coated film confirmed the presence of amorphous PCBM and the absence of crystalline PCBM (Fig. 4a). The TEM images are in agreement with the recorded electron diffraction patterns of the same sample, which only feature a broad halo that is characteristic for amorphous material. In contrast, films annealed above T_g^{blend} display distinct PCBM aggregates surrounded by a depletion zone (see Fig. 4b and d for TEM; Fig. S2† for SEM). Electron diffraction patterns, which are consistent with previous reports,[14,15] indicate that these aggregates are single-crystal-like entities. In addition, we examined the area in between crystals (Fig. 4c). Electron diffraction only reveals a broad halo, which suggests that no crystalline PCBM is present.

We were able to observe the degree of phase separation, which could be resolved with TEM and SEM as well as atomic force microscopy (AFM; Fig. S3†). We find good agreement with our previous electron tomography study that permitted determination of not only the size but also makeup of domains.[30] We thereby conclude that in the here studied spin-coated samples the PCBM-rich amorphous domains, which are about 50 nm in diameter, are surrounded by TQ1-rich material. Moreover, this nanostructure appears to be independent of the choice of substrate (*cf.* Fig. S2†). Annealing results in a coarsening of the blend nanostructure that is characterised by larger PCBM domains with a diameter of about 100 nm (Fig. 4b–d). Instead,

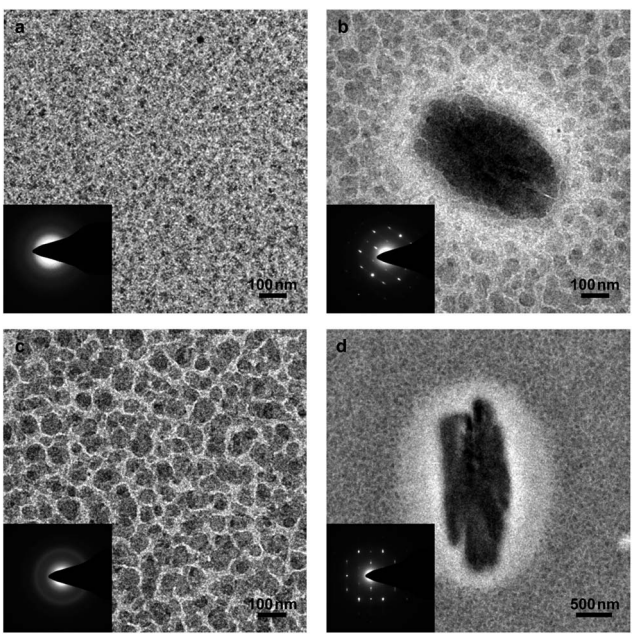

Fig. 4 TEM micrographs and electron diffraction patterns (insets) of 1 : 1 TQ1:PCBM films: (a) pristine, spin-coated (b and c) annealed at 130 °C and (d) annealed at 150 °C.

the depletion zone, which develops around PCBM crystals and is several 100 nm wide, appears to be predominately composed of the TQ1-rich phase (Fig. 4b and d and S2b and d†). Previous reports have argued that this feature arises because PCBM from the adjacent blend is consumed during crystal growth.[15,17] The consumption of PCBM is corroborated by the noticeable decrease in film thickness by up to ~10 nm within the depletion zone, *i.e.* ~11% of the total film thickness (measured with profilometry; Fig. S4†). In contrast, AFM images suggest that the actual PCBM crystals protrude from the blend film by at least 100–300 nm, which depends on the annealing time $\Delta t_{\mathrm{anneal}}$ and temperature T_{anneal} (Fig. S3 and S4†).

We recorded high-magnification optical micrographs of TQ1:PCBM films in between discrete isothermal annealing steps to extract information about the size and number of PCBM crystals as a function of $\Delta t_{\mathrm{anneal}}$. Whereas the width W of PCBM crystals rapidly reached a constant value, their length L continued to increase with $\Delta t_{\mathrm{anneal}}$. Thus, the aspect ratio L/W reached a higher value in particular at elevated T_{anneal} (Fig. S5†). We used L as a proxy for the amount of crystallised material. L initially increased linearly with $\Delta t_{\mathrm{anneal}}$ but eventually approached a maximum value due to impingement of PCBM crystals or, potentially, the surrounding depletion zone. We extracted the initial growth rate $\dot{L}$ from straight line fits to the linear region of our experimental data (Fig. 5a):

$$\dot{L} = \frac{\Delta L}{\Delta t_{\mathrm{anneal}}} \quad (1)$$

Reassuringly, for samples annealed at 110 °C we could confirm that optical microscopy and SEM yield comparable values (Fig. S6†). We repeated the optical microscopy analysis for a series of annealing temperatures from 110 and 230 °C to obtain $\dot{L}(T)$. In this temperature range, we find that $\dot{L}(T)$ increases by over two orders of magnitude. Classical crystallisation theory offers a straightforward expression for diffusion-limited growth, which occurs close to T_g.[31] The Stokes–Einstein relation can be used to describe the diffusion coefficient D:

$$D = \frac{kT}{6\pi a\eta} \quad (2)$$

where k is the Boltzmann constant and a the particle radius. Close to T_g, the viscosity η can be described according to the Vogel–Fulcher–Tammann equation:

$$\eta = \eta_0 e^{\frac{A}{T-T_f}} \quad (3)$$

where η_0, A and T_f are constants. Thus, by considering proportionality between $\dot{L}(T)$ and D, we obtain:

$$\dot{L}(T) \propto Te^{-\frac{A}{T-T_f}} \quad (4)$$

As can be discerned from Fig. 5b, this expression provided a good fit to our experimental data, which suggests that across the studied temperature range PCBM crystal growth is indeed diffusion limited. Moreover, our analysis suggests that the diffusion constant of PCBM in TQ1 varies by two orders of magnitude between 110 °C and 230 °C. At higher temperatures that approach T_m^{PCBM} we expect $\dot{L}(T)$ to decrease again. In fact, our DSC measurements indicate that the onset of melting occurs at as low as 250 °C (*cf.* Fig. 2a).

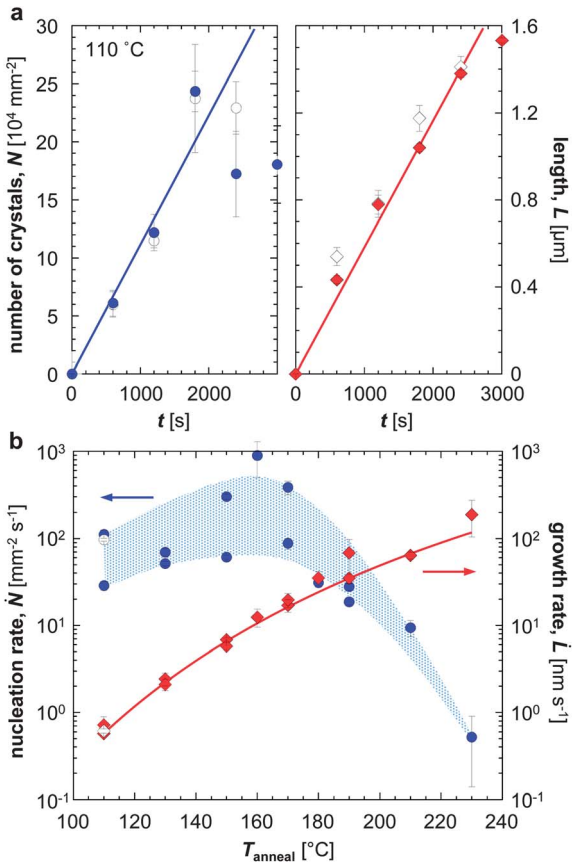

Fig. 5 (a) Number (left) and length of crystals (right) from optical micrographs (filled) and SEM images (open) for a 1 : 1 TQ1:PCBM film spin-coated on a glass substrate and annealed at 110 °C. The nucleation and crystal growth rate, $\dot{N}$ and $\dot{L}$, are estimated from the slope of the linear fits (solid lines). Error bars reflect standard deviations based on comparison of 5–10 discrete optical micrographs or subsections of the same SEM image. (b) $\dot{N}$ (blue circles) and $\dot{L}$ (red diamonds) as a function of annealing temperature T_{anneal} extracted from optical micrographs (filled symbols) and for 110 °C also from SEM images (open symbols). Error bars reflect standard deviations of linear fits to the number of nuclei and length of crystals, respectively (*cf.* (a)). The growth rates were fitted with eqn (4) (red line).

Evaluation of the same high-magnification optical micrographs of isothermally annealed TQ1:PCBM films offered an estimate of the number N of PCBM crystals. Again, an initial linear region is followed by a sub-linear behaviour (Fig. 5a). Optical and SEM images of samples annealed at 110 °C are in good agreement, which confirms that optical microscopy is sufficient to accurately track the amount of PCBM crystals. The gradient of straight line fits to the initial linear region provided a measure for the nucleation rate $\dot{N}$:

$$\dot{N} = \frac{\Delta N}{\Delta t_{\mathrm{anneal}}} \quad (5)$$

Across the studied temperature range of 110–230 °C we notice that $\dot{N}(T)$ considerably varies when comparing measurements of different samples that have experienced the same annealing protocol. For instance, we examined two samples at $T_{\mathrm{anneal}} \sim 110$ °C, which yielded $\dot{N} \sim 29 \pm 3$ mm^{-2} s^{-1}

and 111 ± 14 mm^{-2} s^{-1}. It is likely that variations in surface roughness or contamination alter the number of nucleation events. Unfortunately, this considerable spread in $\dot{N}(T)$ prevented us from reliably fitting our experimental data. Thus, we limit the discussion to a qualitative analysis. According to classical crystallisation theory the rate of nucleation is governed by:[31]

$$\dot{N}(T) \propto \omega e^{-\frac{\Delta G^*}{kT}} \quad (6)$$

Here, ω is the frequency of attachment of molecules to the critical nucleus and ΔG^* is the Gibbs free energy that is needed for formation of a critical nucleus with radius r^*:

$$\Delta G^* \propto r^{*2} \propto \frac{1}{\left(T - T_m^{PCBM}\right)^2} \quad (7)$$

Close to T_g nucleation is diffusion-limited and ω can be described with eqn (2) and (3), which implies that $\dot{N}(T)$ decreases strongly at low temperatures. Similarly, for higher temperatures the degree of undercooling is reduced, that is T_{anneal} approaches T_m^{PCBM}. As a result the exponential Boltzmann factor, which depends on ΔG^*, becomes small. Thus, we expect a maximum $\dot{N}(T)$ at intermediate temperatures. Indeed, as revealed by Fig. 5b, $\dot{N}(T)$ has a broad maximum around $T_{anneal} \sim 150$–170 °C. Thus, we conclude that for $T_{anneal} < 150$ °C, PCBM nucleation is diffusion limited. Instead, for $T_{anneal} > 170$ °C the free energy of formation of a critical nucleus increases and thus $\dot{N}(T)$ drops by three orders of magnitude from a value as high as 890 ± 400 mm^{-2} s^{-1} to a much lower 0.5 ± 0.4 mm^{-2} s^{-1}.

We could predict the initial relative rate of crystallisation $\dot{C}$ by considering that after an annealing time Δt_{anneal} there are $\dot{N}\Delta t_{anneal}$ crystals present that grow in length at rate $\dot{L}$:

$$\dot{C} \propto \dot{N}\Delta t_{anneal}\dot{L} \quad (8)$$

We used experimentally found values for $\dot{N}$ and $\dot{L}$ to calculate $\dot{C}$ (Fig. 6a). A maximum $\dot{C}$ around $T_{anneal} \sim 160$–170 °C is in reasonable agreement with our DSC measurements, which indicate that re-crystallisation of PCBM during heating of TQ1:PCBM blends peaks at 175 °C (*cf.* Fig. 2a).

Finally, in order to illustrate the relative contribution of nucleation and growth to the formation of PCBM crystals, we constructed a time-temperature-transformation (TTT) diagram (Fig. 6b). The TTT diagram displayed in Fig. 6b can be used to predict the number and length of crystals that result from different annealing protocols. In the following, we consider annealing at $T_{anneal} \sim 170$ °C, which is close to the peak DSC re-crystallisation temperature. At this temperature we find $\dot{L} \sim 20$ nm s^{-1} and $\dot{N} \sim 88$–385 mm^{-2} s^{-1}. Thus, we extrapolate that after $\Delta t_{anneal} \sim 1$ s approximately 10^2 PCBM crystals are present per mm^2, the largest of which are 20 nm long. Further annealing results in a considerably larger number of 10^3 crystals per mm^2 after $\Delta t_{anneal} \sim 3$–11 s. At this point of time, the biggest crystals tend to be more than 100 nm long. From our isothermal annealing experiments we conclude that at 170 °C the initial linear regime of $L(t)$ and $N(t)$ extends to $\Delta t_{anneal} \sim 300$ s (Fig. S7†), after which impingement of crystals occurs. At this point only 0.03–0.12 crystals are present per μm^2, of which the largest ones have already reached a length of 6 μm. Clearly, the low nucleation rate of PCBM crystals in the here investigated TQ1:PCBM blend limits the growth of sufficiently small structures.

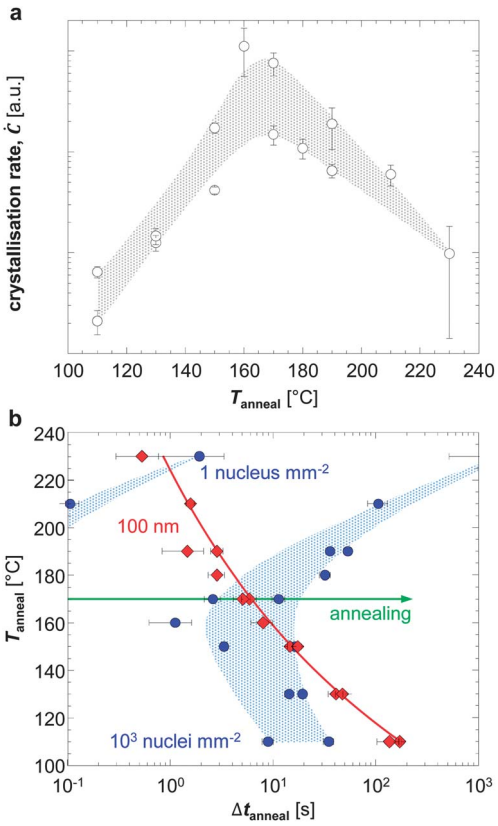

Fig. 6 (a) The overall crystallisation rate after annealing time Δt_{anneal}, which is proportional to the product of $\dot{N}\Delta t_{anneal}$ and $\dot{L}$, and (b) corresponding time-temperature-transformation (TTT) diagram indicating progress of nucleation (blue circles) and growth (red diamonds). The green arrow indicates isothermal annealing at 170 °C.

3 Conclusions

We have studied the nucleation and growth of PCBM crystals in thin films of the polymer:fullerene bulk-heterojunction blend TQ1:PCBM. PCBM crystallisation, which commenced by heterogeneous nucleation on the glass substrate, was monitored with optical microscopy over a wide temperature range of 110–230 °C. SEM and TEM were used to further investigate the annealed material. At lower temperatures, which approach the T_g of the blend components, we found that both nucleation and growth are strongly diffusion limited. The growth rate exponentially increased with temperature. In contrast, the nucleation rate displayed a maximum around 150–170 °C, which resulted in the highest rate of PCBM crystallisation at these temperatures. Moreover, we constructed a time-temperature-transformation (TTT) diagram, which revealed that the low overall rate of nucleation encourages the growth of micrometre-sized PCBM crystals across the investigated temperature range.

4 Experimental

Materials

PCBM (purity >99%) was purchased from Solenne BV. TQ1 was prepared according to previously published procedures ($M_n \sim 56$ kg mol^{-1}, $M_w \sim 170$ kg mol^{-1}).[22]

Thin film preparation

Solutions were filtered with a 0.45 μm PTFE filter prior to spin-coating. Thin films were spin-coated from a solution of TQ1:PCBM in chlorobenzene (1 : 1 ratio with a total concentration of 20 g L^{-1}) on glass substrates (cleaned by sonicating in acetone and then isopropanol followed by rinsing with water, acetone, dichloromethane and then isopropanol) or poly(3,4-ethylenedioxythiophene):poly(styrenesulfonate) (PEDOT:PSS; Heraeus, Clevios P VP Al 4083) coated glass substrates. The film thickness was ~90 nm as measured by AFM. Spin-coated films were allowed to dry for at least 15 hours to remove residual solvents. Annealing was carried out on a Kofler bench at ambient atmosphere but with thorough light protection. The Kofler bench was calibrated with K-type self-adhesive thermocouples from Omega (estimated error ±5 °C; time to reach stable temperature ~30 s).

Differential scanning calorimetry

Measurements were performed under nitrogen at a scan rate of 10 °C min^{-1} with a Perkin Elmer Pyris 1 equipped with a Perkin Elmer Intra cooler 1P.

UV-Vis absorption spectroscopy

Measurements were performed with a Perkin Elmer Lambda 900 UV-Vis-NIR spectrophotometer.

Optical microscopy

Optical micrographs were taken in reflection mode with an Olympus BH-2 microscope equipped with an Olympus DP12 camera system.

Contact angle measurements

Water contact angles were measured with a DAT1100 from Fibro System AB. The data were collected *via* the software Dynamic Absorption Tester DAT 3.6.

Transmission electron microscopy

Micrographs and diffraction patterns were obtained with a J2 G2 Tecnai TEM operated at an acceleration voltage of 200 kV. Samples were prepared by floating off spin-coated films on PEDOT:PSS coated glass substrates in water, followed by collection with TEM copper mesh grids.

Scanning electron microscopy

Measurements were done with a Leo Ultra 55 SEM equipped with a field emission gun (LEO Electron Microscopy Group, Germany) and a secondary electron detector. The acceleration voltage was 3 kV. Both, samples coated with a 10 nm gold layer and without any conducting layer were imaged.

Atomic force microscopy

Measurements were done with a Digital Instrument Nanoscope IIIa equipped with a type G scanner (Digital Instrument Inc., Santa Barbara, CA, USA). The measurements were done in tapping mode and in air using a Micro Masch NSC 15 silicon cantilever.

Profilometry

The measurements were carried out on a KLA Tencor P-15 programmable stylus surface profiler system.

Acknowledgements

We acknowledge the Swedish Research Council, Swedish Energy Agency, Formas as well as Chalmers' Areas of Advance Energy, Materials Science and Nanoscience and Nanotechnology for funding. C.L. is supported by the Linnaeus Centre for Bioinspired Supramolecular Function and Design (SUPRA). We thank Dr. Mattias Eng (Chalmers) for help with profilometry measurements.

References

1 G. Yu, J. Gao, J. C. Hummelen, F. Wudl and A. J. Heeger, *Science*, 1995, **270**, 1789–1791.
2 J. J. M. Halls, C. A. Walsh, N. C. Greenham, E. A. Marsegila, R. H. Friend, S. C. Moratti and A. B. Holmes, *Nature*, 1995, **376**, 498–500.
3 R. A. J. Janssen and J. Nelson, *Adv. Mater.*, 2012, **25**, 1847–1858.
4 E. Verploegen, R. Mondal, C. J. Bettinger, S. Sok, M. F. Toney and Z. Bao, *Adv. Funct. Mater.*, 2010, **20**, 3519–3529.
5 J. Zhao, A. Swinnen, G. V. Assche, J. Manca, D. Vanderzande and B. V. Mele, *J. Phys. Chem. B*, 2009, **113**, 1587–1591.
6 C. Müller, J. Bergqvist, K. Vandewal, K. Tvingstedt, A. S. Anselmo, R. Magnusson, M. I. Alonso, E. Moons, H. Arwin, M. Campoy-Quiles and O. Inganäs, *J. Mater. Chem.*, 2011, **21**, 10676–10684.
7 F. Padinger, R. S. Rittberger and N. S. Sariciftci, *Adv. Funct. Mater.*, 2003, **13**, 85–88.
8 T. J. Savenije, J. E. Kroeze, X. Yang and J. Loos, *Adv. Funct. Mater.*, 2005, **15**, 1260–1266.
9 X. Yang, J. Loos, S. C. Veenstra, W. J. H. Verhees, M. M. Wienk, J. M. Kroon, M. A. J. Michels and R. A. J. Janssen, *Nano Lett.*, 2005, **5**, 579–583.
10 C. Müller, T. A. M. Ferenczi, M. Campoy-Quiles, J. M. Frost, D. D. C. Bradley, P. Smith, N. Stingelin-Stutzmann and J. Nelson, *Adv. Mater.*, 2008, **20**, 3510–3515.
11 International standard ASTM E 1171 requires thermal stability testing of solar cells at a temperature of 85 °C.
12 B. Conings, S. Bertho, K. Vandewal, A. Senes, J. D'Haen, J. Manca and R. A. J. Janssen, *Appl. Phys. Lett.*, 2010, **96**, 163301.

13 D. Chirvase, J. Parisi, J. C. Hummelen and V. Dyakonov, *Nanotechnology*, 2004, **15**, 1317–1323.
14 X. Yang, A. Alexeev, M. A. J. Michels and J. Loos, *Macromolecules*, 2005, **38**, 4289–4295.
15 X. Yang, J. K. J. van Duren, R. A. J. Janssen, M. A. J. Michels and J. Loos, *Macromolecules*, 2004, **37**, 2151–2158.
16 A. Swinnen, I. Haeldermans, M. vande Ven, J. D'Haen, G. Vanhoyland, S. Aresu, M. D'Olieslaeger and J. Manca, *Adv. Funct. Mater.*, 2006, **16**, 760–765.
17 S. Bertho, I. Haeldermans, A. Swinnen, W. Moons, T. Martens, L. Lutsen, D. Vanderzande, J. Manca, A. Senes and A. Bonfiglio, *Sol. Energy Mater. Sol. Cells*, 2007, **91**, 385–389.
18 B. Watts, W. J. Belcher, L. Thomsen, H. Ade and P. C. Dastoor, *Macromolecules*, 2009, **42**, 8392–8397.
19 M. Shin, H. Kim, J. Park, S. Nam, K. Heo, M. Ree, C.-S. Ha and Y. Kim, *Adv. Funct. Mater.*, 2010, **20**, 748–754.
20 C. He, D. S. Germack, R. Joseph Kline, D. M. Delongchamp, D. A. Fischer, C. R. Snyder, M. F. Toney, J. G. Kushmerick and L. J. Richter, *Sol. Energy Mater. Sol. Cells*, 2011, **95**, 1375–1381.
21 W.-R. Wu, U.-S. Jeng, C.-J. Su, K.-H. Wei, M.-S. Su, M.-Y. Chiu, C.-Y. Chen, W.-B. Su, C.-H. Su and A.-C. Su, *ACS Nano*, 2011, **5**, 6233–6243.
22 E. G. Wang, L. Hou, Z. Wang, S. Hellström, F. Zhang, O. Inganäs and M. R. Andersson, *Adv. Mater.*, 2010, **22**, 5240–5244.
23 R. Kroon, R. Gehlhaar, T. T. Steckler, P. Henriksson, C. Müller, J. Bergqvist, A. Hadipour, P. Heremans and M. R. Andersson, *Sol. Energy Mater. Sol. Cells*, 2012, **105**, 280–286.
24 E. G. Wang, J. Bergqvist, K. Vandewal, Z. Ma, L. Hou, A. Lundin, S. Himmelberger, A. Salleo, C. Müller, O. Inganäs, F. Zhang and M. R. Andersson, *Adv. Energy Mater.*, 2013, DOI: 10.1002/aenm.201201019.
25 We did not heat to higher temperatures in order to minimise thermal degradation of PCBM. Previously, we have observed that TQ1 with $M_n \sim 93$ kg mol^{-1} displays a weak endothermic peak at 300 °C, which we associated with a liquid-crystalline to isotropic transition (ref. 24).
26 J. Y. Kim and C. D. Frisbie, *J. Phys. Chem. C*, 2008, **112**, 17726–17736.
27 S. Bertho, G. Janssen, T. J. Cleij, B. Conings, W. Moons, A. Gadisa, J. D'Haen, E. Goovaerts, L. Lutsen, J. Manca and D. Vanderzande, *Sol. Energy Mater. Sol. Cells*, 2008, **92**, 753–760.
28 C. Girotto, D. Cheyns, T. Aernouts, F. Banishoeib, L. Lutsen, T. J. Cleij, D. Vanderzande, J. Genoe, J. Poortmans and P. Heremans, *Org. Electron.*, 2008, **9**, 740–746.
29 A. S. Anselmo, *Materials aspects in spin-coated films for polymer photovoltaics*, Karlstad University, 2013.
30 L. Hou, E. Wang, J. Bergqvist, B. V. Andersson, Z. Wang, C. Müller, M. Campoy-Quiles, M. R. Andersson, F. Zhang and O. Inganäs, *Adv. Funct. Mater.*, 2011, **21**, 3169–3175.
31 J. A. Kalb, in *Phase Change Materials*, ed. S. Raoux and M. Wuttig, 2009, pp. 125–148.

